Optimal Design of a 3.5 kV/11 kW DC-DC Converter for Charging Capacitor Banks of Power Modulators

G. Ortiz, D. Bortis, J. Biela and J. W. Kolar
Power Electronic Systems Laboratory, ETH Zurich
Email: ortiz@lem.ee.ethz.ch

***Abstract*—For the generation of short high power pulses in many applications, power modulators based on capacitor discharge are used, where the peak power is drawn from the input capacitor bank. In order to continuously recharge the energy buffer during operation at a lower average power, usually power supplies connected to the mains are used. Due to the worldwide variation in mains voltages and the desired ability to adapt the capacitor voltage of the modulator, the power supply has to support a wide input and output voltage range, whereby the supply should draw a sinusoidal current from the mains due to EMI regulations. Additionally, depending on the modulator concept, also a galvanic isolation has to be provided. In order to achieve the mentioned specifications for the considered power supply, a combination of a AC-DC and DC-DC converter is proposed, whereas the mains voltage is rectified by a three-phase buck-boost converter to 400Vdc and thereafter an isolated DC-DC converter charges the input capacitor bank of the power modulator up to 3.5 kV. This paper focuses on the basic operation and the design of the 3.5kV/11kW isolated DC-DC converter, which includes transformer design, efficiency-volume optimization and components selection. There, compared to the well-known flyback converter the proposed full-bridge based topology results in a much higher efficiency and power density.**

I. Introduction

Usually, in power modulators based on capacitor discharge, the energy buffer is continuously recharged during operation at a lower average power by a power supply connected to the mains. In order to enable a worldwide operation, the AC-DC converter has to provide a wide input range, which can vary from 177 V to 528 V [1]. Due to this worldwide variation in mains voltages, the desired ability to adapt the capacitor voltage of the modulator from 0 V to 3.5kV, and the specified galvanic isolation between the converter output and the mains, for the power supply a combination of a AC-DC and DC-DC converter is proposed in this paper, as shown in Fig. 1.

There, the mains voltage is rectified by a three-phase buck-boost converter to the voltage V_{in} [1] and thereafter an isolated, full-bridge based DC-DC converter charges the input capacitor bank of the power modulator up to 3.5kV. The voltage V_{in} of the 3.5 kV/11 kW isolated, full-bridge based DC-DC converter is set to 400 Vdc, in order to use 600 V IGBT modules, which show the best performance regarding switching frequency and switching losses at these power levels.

In Table I the nominal specifications of the isolated DC-DC converter are given. Additionally, for the considered application, the isolated DC-DC converter should also be able to deliver the nominal output power of 11 kW when a variation of the input

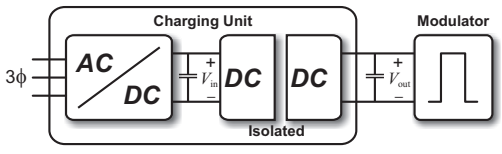

Figure 1: Block diagram of the charging unit, consisting of a three-phase AC-DC and a DC-DC converter, which interconnects the power modulator to the mains.

TABLE I: Specifications of the isolated DC-DC converter.

Parameter	Nominal value	Incl. range
Input voltage V_{in}	400 V	350...450 V
Output voltage V_{out}	3500 V	3150...3850 V
Max output power P_{out}	11 kW	15 kW
Switching frequency f_s=1/T_s	30 kHz	–

and output voltage of $\pm 10\,\%$ is taken into account, which results at the nominal operating point in a maximum output power of 15 kW (cf. Table I).

This paper focuses on the operation and the design of the 3.5 kV/11 kW isolated, full-bridge based DC-DC converter, which includes the design of a high-frequency transformer, efficiency-volume optimization of the converter and the components selection like semiconductor switches or core materials. In **Section II** the basic operation principle of the full-bridge based converter is explained in detail. This operation is later translated into a converter model described by analytic equations in **Section III**. With these equations, in **Section IV** the DC-DC converter is optimized for minimal volume/losses. Also in this section, the construction of the transformer/converter is presented whereas the resulting design performance and experimental results are presented in **Section V**. As will be shown in Section V, compared to the well-known two-switch flyback converter [2, 3] the proposed full-bridge based DC-DC converter results in a much higher efficiency and power density.

II. Converter Operation

In this section the basic operation and the modulation of the full-bridge based DC-DC converter, shown in Fig. 2, are explained in detail. Additionally, the design equations of the DC-DC converter will be derived for the main components like transformer and semiconductors. Thereafter, the design of the converter can be optimized concerning efficiency and power density.

A. Topology

The considered full-bridge topology (cf. Fig. 2) can be divided into three parts: the input stage, the HF-transformer and the rectifier stage. The inverter stage, which is a full-bridge configuration, consists of the four switches $T_1 - T_4$. At the input the full-bridge is connected to the DC voltage V_{in} (cf. Fig. 2). In order to provide the galvanic isolation and to step-up the input voltage V_{in}, a transformer is required. In addition to the transformer a series inductance is needed to enable the power transfer and to ensure soft switching of the four switches. The rectifier stage consists of the two diodes D_1 and D_2 as well as of the two capacitors C_1 and C_2. There, the diodes D_1 and D_2 must be able to block the whole output voltage V_{out}, whereas the capacitors C_1 and C_2 are only charged to the half of the output voltage V_{out} (voltage doubler).

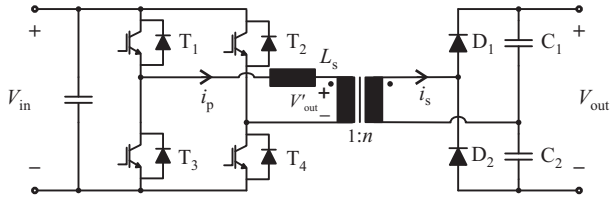

Figure 2: Schematic of the isolated, full-bridge based DC-DC converter.

B. Basic operation principle

The operation of the full-bridge based DC-DC converter is now described upon the waveforms shown in Fig. 3.

In order to enable power transfer, the input voltage V_{in} has to be larger than the reflected output voltage $V'_{out} = V_{out}/2n$. In this case, when T_1 and T_4 are switched-on at the beginning of one switching cycle, the voltage at the output of the full-bridge equals the DC voltage V_{in} and due to $V_{in} > V_{out}/2n$ the diode D_1 starts to conduct. Consequently, at the transformer's input terminals the voltage V'_{out} is clamped to $V_{out}/2n$. Therefore, the difference between the reflected voltage V'_{out} and the DC input voltage V_{in} is applied to the series inductance L_s. If constant input and output voltages are assumed, this leads to a linearly increasing current $i_{p1}(t)$ through the series inductance L_s and the load (cf. Fig. 3).

$$i_{p1}(t) = n \cdot i_{s1}(t) = \frac{V_{in} - V_{out}/(2n)}{L_s} t \tag{1}$$

At the time instant DT_s the transistor T_1 is turned off and the current i_{p1} commutates to the antiparallel diode of T_3. After a certain interlocking delay the switch T_3 can be turned on, whereby soft switching (ZVS) is achieved. Consequently, the voltage at the output of the full-bridge is zero and the reflected output voltage V'_{out} is fully applied to the series inductance L_s, which results in a linearly decreasing current $i_{p2}(t)$ (cf. Fig. 3).

$$i_{p2}(t) = i_{s2}(t)n = i_{1p}(DT_s) - \frac{V_{out}/(2n)}{L_s} t \tag{2}$$

In the following, the converter is operated in discontinuous conduction mode, which means that the current $i_{p2}(t)$ will reach zero before $t = T_s/2$. Thereby, the current $i_{p2}(t)$ stays at zero

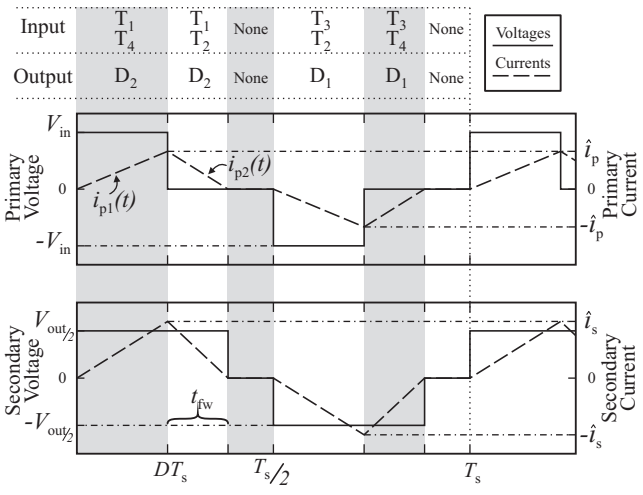

Figure 3: Qualitative operation waveforms of the full-bridge based DC-DC converter.

until the second half period is started at $T_s/2$ and switch T_4 can be turned off. The operation during $T_s/2 - T_s$ is analogous to $0 - T_s/2$, whereas, in order to obtain a negative primary current, the switches T_2 and T_3 are turned on. Accordingly, at $T_s/2 + DT_s$ switch T_3 is turned off and T_1 is turned on. There, only the reflected output voltage V'_{out} is applied to the transformer, which results in a linearly increasing current until it reaches zero.

III. Converter Model

The first step in the design flow is to consider the design conditions shown in Table I. The degrees of freedom must be identified which in this case are: the turns ratio n, the transformer core geometry, the characteristics of the copper in primary and secondary regarding thickness or diameter.

A model of the losses in the semiconductors and in the transformer is now necessary to choose the appropriate values for each of the degrees of freedom. The first equations to be considered are (1) and (2). Equations to obtain the value of the duty cycle, the series inductance, the transformer losses and the semiconductors losses will be determined now.

A. Duty cycle

The described operation of the full-bridge converter allows to obtain an expression for the required duty cycle D depending on the operation conditions and the construction parameters.

Assuming discontinuous conduction mode, the freewheeling time t_{fw}, in which the current i_{p2} decreases towards zero, can be deduced from (1) and (2).

$$\begin{aligned} & i_{p2}(t_{fw}) = i_{p1}(DT_s) - \frac{V_{out}/(2n)}{L_s} t_{fw} = 0 \\ \Rightarrow \quad & t_{fw} = \frac{V_{in} - V_{out}/(2n)}{V_{out}/(2n)} DT_s \end{aligned} \tag{3}$$

Therewith, the output average current $\bar{I}_{out}$ can be calculated by integrating the output current $i_s(t)$, which is given by the primary current i_{p1} respectively i_{p2} and the turns ratio n.

$$\begin{aligned} \bar{I}_{out} &= \frac{1}{T_s} \left(\int_0^{DT_s} \frac{i_{p1}(t)}{n} dt + \int_0^{t_{fw}} \frac{i_{p2}(t)}{n} dt \right) \\ &= \frac{1}{2} \frac{(2V_{in}n - V_{out}) V_{in} T_s}{n V_{out} L_s} D^2 = \frac{P_{out}}{V_{out}} \end{aligned} \tag{4}$$

Hence, for a given output power P_{out} the duty cycle D can be obtained.

$$\begin{aligned} D &= \frac{\sqrt{2V_{in}(2V_{in}n - V_{out})(1/T_s)nL_s}}{V_{in}(2V_{in}n - V_{out})} \sqrt{P_{out}} \\ &= K \cdot \sqrt{P_{out}} \end{aligned} \tag{5}$$

B. Series Inductance

The value of the series inductance L_s has to be kept below a certain value, since the converter will be operated in the discontinuous conduction mode within the whole operating range. Therefore, the sum of the duration of the duty cycle time DT_s and the freewheeling time t_{fw} has to be shorter than the $T_s/2$, whereas the parameter $k = 0.95$ is used to establish an operation margin.

$$DT_s + t_{fw} = k \frac{T_s}{2} < \frac{T_s}{2} \tag{6}$$

Using (3), (5) and (6) the expression for the series inductance L_s can be determined.

$$L_s = \frac{1}{32}\frac{T_s k^2 V_{out}^2 (2V_{in}n - V_{out})}{V_{in} P_{out} n^3} \tag{7}$$

As can be seen from (7), the value of the series inductance L_s depends on the turns ratio n. As already mentioned, in order to enable power transfer, the input voltage V_{in} has to be larger than the reflected output voltage V'_{out}, which is $V_{out}/2n$. Considering the specifications given in Table I this results in a minimum turns ratio of $n_{min} = 6$. However, since for the following converter design the series inductance L_s will be partly integrated into the transformer, a final transformer design is necessary.

C. Transformer losses model

In order to determine the number of turns N_{pri} and the turns ratio n, the transformer will be optimized regarding the minimum transformer losses. There, the copper losses due to skin and proximity effects as well as the core losses have to be taken into account.

For the converter operation described previously, the maximum flux density $\hat{B}$ can be found with the voltage-time product during the interval $0 - T_s/2$, where A_e is the effective cross-section.

$$\hat{B} = \frac{V_{in} D T_s}{2 N_{pri} A_e} + \frac{V_{out} t_{fw}}{4 N_{pri} A_e n} \tag{8}$$

The expression in (8) can now be solved for the number of turns N_{pri} in the primary, which yields:

$$N_{pri} = \frac{2V_{in} D T_s + V_{out} t_{fw}}{4 \hat{B} A_e} = \frac{N_{sec}}{n} \tag{9}$$

Using (9), for a given transformer/core geometry the resulting conduction losses in the primary and secondary due skin and proximity effects can now be calculated either for foils depending on the foil thickness or for litz wires depending on the litz diameter and the number of strands [4, 5].

The core losses are calculated by using the Steinmetz equation for non-sinusoidal waveforms [6], whereas the Steinmetz parameters are extracted from the core manufacturer's datasheets.

D. Semiconductors losses model

In order to determine the switching and conduction losses of the IGBT modules and the diodes, data regarding output characteristics, turn-off energy, and reverse recovery, in the case of the diodes, is necessary. For the calculation of the switching losses only the hard switching transitions are considered. According to the converter operation explained in section II, hard switching occurs during turn-off for switch T_1 at DT_s respectively for switch T_3 at $T_s/2 + DT_s$. Therefore, only two hard switching transitions have to be considered during one switching period (cf. (10)). Additionally, the duration of conduction for each switch is assumed to be equal, which results in four times the conduction losses of one switch (cf. (11)).

$$P_{sw} = 2E_{off}(\hat{I}_C, v_{CE}) \cdot f_s \tag{10}$$

$$P_{con} = 4\frac{1}{T_s}\int_0^{T_s} v_{CE}(I_C(t)) \cdot I_C(t) dt \tag{11}$$

There, $E_{off}(\hat{I}_C, v_{CE})$ is the hard switching turn-off loss energy for a given collector current $\hat{I}_C$ and collector-emitter voltage v_{CE}. This information as well as the output characteristic $v_{CE}(I_C)$ is extracted from the IGBT datasheet.

Accordingly, the conduction losses for the output diodes are calculated in a same way as for the switches and the reverse recovery losses were calculated as described in [7].

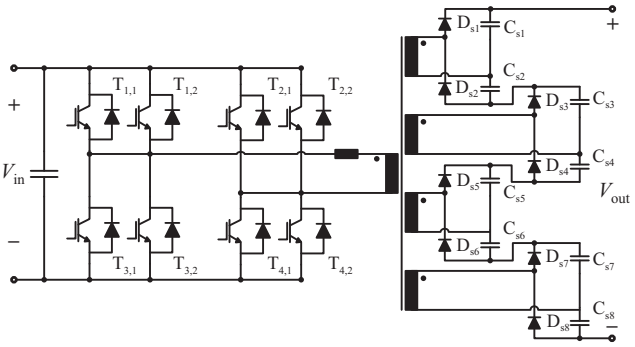

Figure 4: Full-bridge converter with paralleled input IGBTs and split secondary windings.

IV. Converter Design and Construction

Since the converter should operate in a wide power and voltage range (cf. Table I), different components of the converter have to be designed for different operating points, where their critical conditions are encountered. For example, in order to be able to transfer the specified power and to solely operate the converter in DCM, the series inductance has to be designed for the lowest input voltage and the highest output voltage, because in this point the lowest voltage is applied to the inductance. On the other hand, the highest input voltage results in highest semiconductor's losses as in this operating point the highest peak currents are obtained. Therefore, also the heat sink for these components should be designed for the same operating point. Consequently, a wide operating range reduces the maximum reachable efficiency and power density, since not all components can be optimized for a single operating point.

A. Parameter Optimization and Design

Due to stringent requirements regarding high converter efficiency, a HF-transformer concept employing E 80/38/20 N87 E-cores is selected. Ferrite core material is used, since it shows excellent high-frequency performance and enables a compact transformer design. In order to achieve the needed core area A_e, a certain number of core pairs N_{set} have to be stacked. For the primary a 35 mm wide copper foil and for the secondary a litz wire are employed. Due to the high output voltage, the output stage of the converter is built using four series connected rectifiers, whereas each rectifier is connected to an independent secondary winding as shown in Fig. 4. This results in a maximum output voltage of 963 V per diode respectively 482 V per capacitor. Additionally, in the transformer design the four secondary windings are embedded in a chambered bobbin in order to perform proper isolation (cf. Fig. 6-b)).

Depending on the number of core pairs N_{set}, the turns ratio n, the copper foil thickness $d_{cu,p}$, and the secondary litz diameter $d_{cu,s}$ the converter can now be optimized regarding a low loss design in the whole operating range with the given transformer geometry.

According to Fig. 5 for the given specifications (cf. Table I), the lowest loss design, with respect to the whole operation range, is obtained for $n = 7$ and $N_{set} = 4$. For a maximum flux density of $\hat{B} = 250\,\mathrm{mT}$, the number of turns for the primary and secondary is given with (9) to $N_p = 7$ and $N_s = 49$.

Considering (7), this leads to a maximum allowed series inductance of $L_s = 7.93\,\mu\mathrm{H}$, in order to operate the converter solely in DCM. Hence, using (1) and (5), the resulting peak current at DT_s for maximum input voltage and maximum power equals $\hat{i}_p = 151\,\mathrm{A}$ for the primary, respectively $\hat{i}_s = 18\,\mathrm{A}$ for

the secondary. With this configuration the optimal foil thickness of the primary winding is $d_{cu,p} = 100\,\mu\text{m}$. The optimal litz wire of the secondary winding consists of 420 strands with a diameter of $d_{cu,s} = 71\,\mu\text{m}$ (Pack RUPALIT) [8].

Since the converter optimization is mainly determined by the transformer losses, for the switches and diodes, semiconductor devices with low switching respectively low reverse recovery losses have been selected.

There, for each half bridge ($T_1\&T_3$ respectively $T_2\&T_3$) two parallel connected (cf. Fig. 4) 600 V half bridge IGBT-modules with non punch through technology and positive temperature coefficient (Vishay GB100TS60NPbF) are used, whereas each module can handle 40 Adc at 100 C°. For the output rectifiers fast recovery diodes (IXYS DSEP 8-12A) with a blocking capability of 1200 V and a DC current of 10 A were selected.

Due to the high current ripple, for the voltage stabilization at the input and output, film capacitor are employed, where the allowed maximum voltage ripple is specified to $\pm 5\,\%$. This results in a total input and output capacitance of 200 µF respectively 170 nF. As a result of the series connection of four output rectifiers, which leads to a series connection of eight output capacitors, for each capacitor a value of 1.36 µF is needed, so 1.5 µF is suitable.

In order to partly integrate the series inductance L_s into the transformer, the leakage inductance was calculated as described in [9, 10]. The maximum achievable leakage inductance for the given transformer geometry is $L_{lk} = 2.09\,\mu\text{H}$, which is $5.84\,\mu\text{H}$ less than the required series inductance L_s. For that reason, an additional pair of E-cores was added to the transformer, whereas the complete secondary and part of the primary ($N_{p,add}$) are wound around the additional cores (cf. Fig. 6-c)). The inductance in this core is given by:

$$L_{add} = \frac{1}{2}\frac{A_g \mu_0 (N_p - N_{p,add})^2}{g} \tag{12}$$

where g is the air gap between the two additional E cores. Considering the additional inductance ($L_{add} = 5.84\,\mu\text{H}$) and $N_{p,add} = 2$, (12) can be solved for g, obtaining a required air gap of $g = 1.2\,\text{mm}$.

In Table II the design values of the optimized full-bridge based converter are summarized.

B. Transformer Construction

The construction of the designed transformer is one of the most critical tasks within the converter. Special care was taken regarding isolation, series inductance integration and cooling of the internal parts, issues that will be now addressed. 3D CAD drawings of the designed transformer are displayed in Fig. 6, which will be used as reference for the transformer construction description.

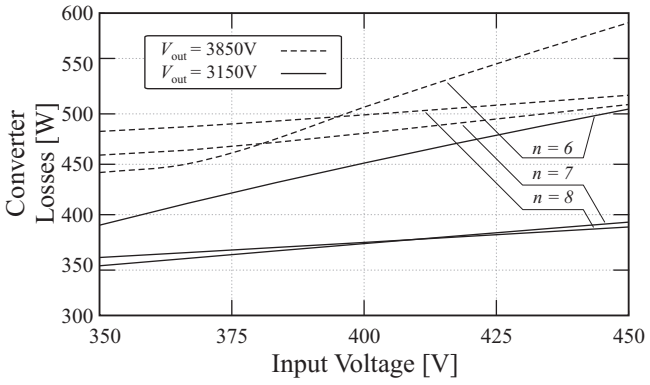

Figure 5: Overall losses for different output voltages and turns ratio.

TABLE II: Design values of the optimized full-bridge converter.

Parameter	Value
Series inductance L_s	7.93 µH
Maximum primary RMS current i_p, rms	58 A
Maximum primary peak current $\hat{i}_p$	151 A
Maximum IGBT losses $P_{M,tot}$	253 W
Maximum output diodes losses $P_{D,tot}$	71 W
Core material	E80/38/20 N87 E core
Number of cores pairs N_{set}	4+1
Air gap between additional cores g	1.2 mm
Maximum flux $\hat{B}$	250 mT
Turns ratio n	7
Turns primary N_p	7
Turns secondary N_s	49
Secondary windings	4
Pri. foil width/thickness $c_{cu,p}$ / $d_{cu,p}$	35 mm / 0.1 mm
Sec. litz number/diameter n_{ls} / $d_{cu,s}$	420 / 0.71 mm
Transformer volume	0.616 dm^3
IGBT module	Vishay GB100TS60NPbF
Output diodes	IXYS DSEP 8-12A
Input capacitor type/capacitance	Film / 200 µF
Output capacitor type/capacitance (each)	Film / 8x1.5 µF
Overall volume	9 dm^3

1) Isolation: To provide the isolation from the primary winding to the core, a 2 mm thick, square-shaped bobbin built with EPOX material is inserted in the middle leg of each pair of E cores (cf. Fig. 6-a)-c)). This material has a 40 kV/mm dielectric strength and a maximum operating temperature of 155 °C. Around this bobbin, the primary foil is wound. A 3 kV isolation between each primary winding turn is provided by a two-sided adhesive interface with a 0.8 W/m-C° thermal conductivity.

As presented in Section IV-A, the transformer output consists of four secondaries, whereas the voltage between two secondary windings is 963 V maximum. Due to this high voltage ratings, each of these secondaries must be properly isolated from each other, from the core and from the primary winding. To do this, the secondary windings were placed into isolated chambered bobbins built with polyethylene terephalate (PET) material, as can be seen in Fig. 6-a)-b). The PET material has a dielectric strength of 16 kV/mm and can withstand temperatures of 130 °C.

With this construction, a high power density is reached while the isolation for each of the windings is guaranteed.

2) Series inductance: In Section IV-A, the integration of the series inductance within the transformer was discussed, whereas one additional pair of E-cores was used in order to increase the series inductance (cf. Fig. 6-c)). There, five out of the seven turns of the primary winding foil are wound around the four transformer core pairs and the last two turns are wound around all five core pairs where a gap of g=1.2 mm is placed in the extra core pairs. The secondaries chambered bobbins are also placed around all five core pairs.

3) Cooling concept: To perform proper isolation for the transformer, the four secondary windings and the primary are enclosed by chambered bobbins as shown in Fig. 6. Due to this tight construction, the primary winding is confined to a small unventilated space, whereby a special cooling concept was incorporated. There, the cooling of the primary is achieved by inserting bent copper plates between the primary bobbins and the winding (cf. Fig. 6-a)). These copper pieces conduct the heat to extruded heat sinks on the top and bottom of the transformer.

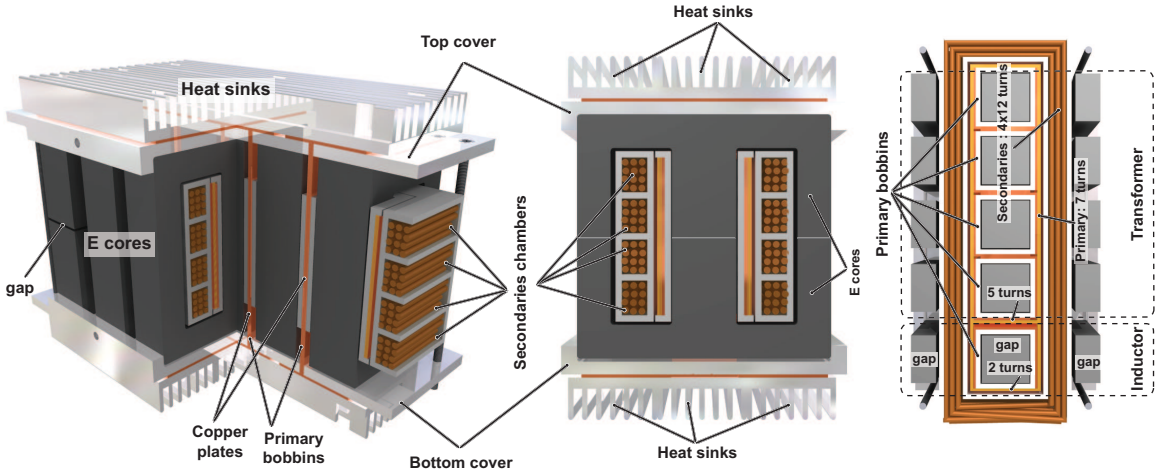

(a) (b) (c)

Figure 6: 3D CAD Transformer cross sections: a) Quarter section view; b) Half front section view.; c) Half top section view.

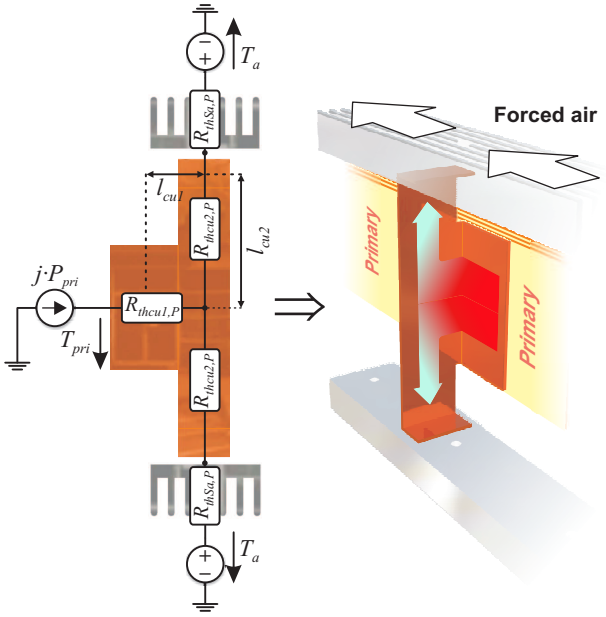

Figure 7: Transformer cooling concept through bent copper plates.

A simple thermal circuit for one of the inserted copper pieces is shown in Fig. 7. The thermal resistances $R_{thcu1,P}$ and $R_{thcu2,P}$ of the copper plate depend on its geometry and can be calculated from:

$$R_{thcu1,P} = \frac{l_{cu1}}{\lambda_{cu} \cdot A_{cu1}} \tag{13}$$

$$R_{thcu2,P} = \frac{l_{cu2}}{\lambda_{cu} \cdot A_{cu2}} \tag{14}$$

where λ_{cu} is the copper's thermal conductivity and A_{cu1} and A_{cu2} are the cross-sections of the paths l_{cu1} and l_{cu2} respectively.

Using this thermal circuit, the required thermal resistance of the top and bottom heat sinks can be calculated with:

$$R_{thsa,P} = \frac{2(T_{pri} - T_a - j \cdot P_{pri} R_{thcu1,P})}{j \cdot P_{pri}} - R_{thcu2,P} \tag{15}$$

where $j \cdot P_{pri}$ represents the power dissipated in the portion of the primary winding in contact with the copper plate.

With the dimensions of the E-cores, we obtain values for l_{cu1} = 27.5 mm and l_{cu2} = 51 mm. Moreover, considering a 1 mm thick copper place, the aforementioned cross-sections are A_{cu1} = 50 mm^2, A_{cu2} = 22.2 mm^2. Then, for a temperature rise of ΔT_P = $T_{pri} - T_a$ = 50 C° at maximum primary copper losses (63 W), the required heat sink's thermal resistance corresponds to $R_{thsa,P}$ = 0.77 °C/W.

To achieve this value, the Fischer SK 177 heat sink was selected. With six 141 mm long heat sinks placed as shown in Fig. 6-b), the overall forced air cooled thermal resistance reaches $R_{thsa,P}$ = 0.51 °C/W. These heat sinks are placed on the top/bottom aluminium covers (cf. Fig. 6-a)-b)) used to enclose the complete transformer.

C. Final Converter Construction

In Fig. 8 a picture of the transformer and the whole designed prototype is shown. The size of the converter is defined by the two 120 mm fans in the front of the converter. One of these fans is attached to a 120x120x200 mm heat sink, on which the four IGBT-modules are mounted. The transformer is placed next to the heat sink, so it receives enough air flow from the second fan. Finally, the converter is covered with the PCB, which comprises the control and measurement electronics as well as the connections for the power electronic components.

V. Converter Performance and Experimental Results

A. Efficiency and Loss Distribution

Based on the design performed in the previous section, the theoretical efficiency of the converter is shown in Fig. 9 considering the whole input and output voltage range at full output power.

The highest efficiency of about 97 % is achieved at lowest input and highest output voltage (V_{in} = 350 V and V_{out} = 3850 V), due to the lowest output current and the lowest peak currents at this operating point. As a result of the increasing peak current for higher input and lower output voltages, the switching losses

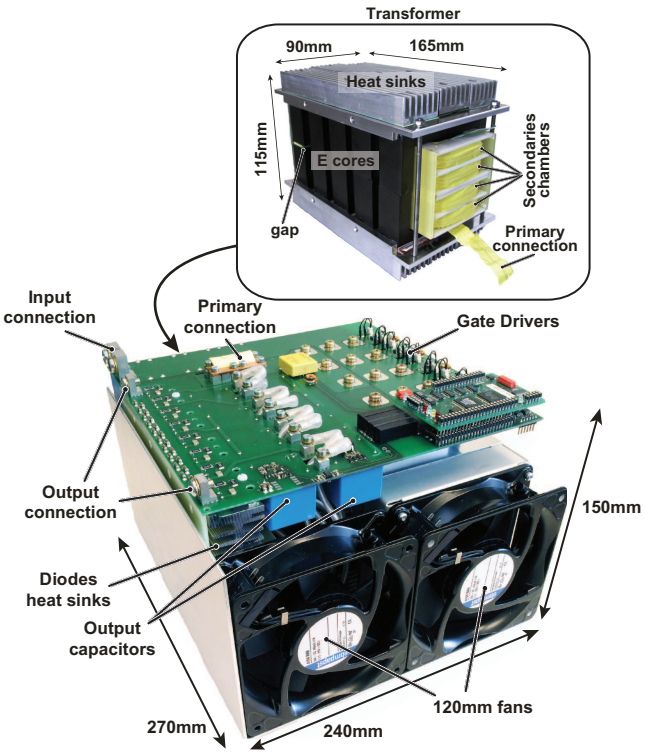

Figure 8: Picture of the designed 3.5 kV/11 kW isolated full-bridge based DC-DC converter and the HF transformer.

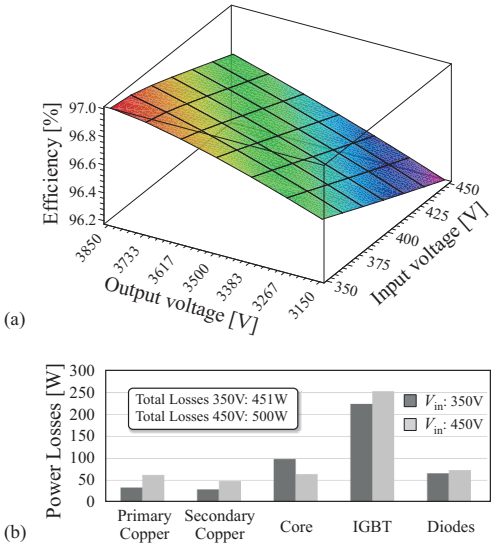

Figure 9: **(a)** Efficiency of the converter in the whole input and output voltage range and **(b)** loss distribution for the two operating points $V_{in} = 350\,\text{V}$, $V_{out} = 3850\,\text{V}$ and $V_{in} = 450\,\text{V}$, $V_{out} = 3850\,\text{V}$ at maximum output power.

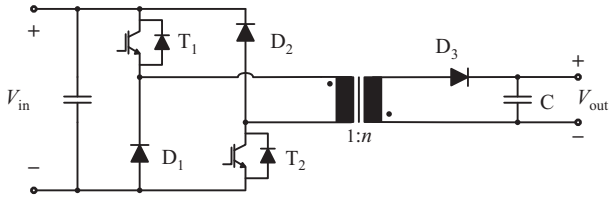

Figure 10: Schematic of the two switch flyback converter.

in the IGBT modules increase about 13 % (35 W) and therefore the efficiency decreases. Due to the same reason, also the copper losses in primary and secondary windings increase. Consequently, in the worst case, at $V_{in} = 450\,\text{V}$ and $V_{out} = 3150\,\text{V}$, an efficiency of around 96.2 % is obtained.

In addition to the efficiency, Fig. 9 shows the loss distribution for the two operating points ($V_{in} = 350\,\text{V}$, $V_{out} = 3850\,\text{V}$ and $V_{in} = 450\,\text{V}$, $V_{out} = 3850\,\text{V}$) at maximum output power. There, it can be seen that the IGBTs contribute with the largest portion of the overall converter losses for either operating point.

In Table III the loss distribution of the optimized full-bridge based converter is summarized. Additionally, compared to the well-known two-switch flyback converter (cf. Fig 10), the proposed full-bridge based topology results in a higher efficiency (96.2 % for the fullbridge and 93.2 % for the flyback) and power density.

The considerable differences observed in peak currents are unavoidable, since the flyback is based on storing energy in the core during DT_s and providing it to the load during t_{fw}, whereas the full-bridge based converter transfers power during DT_s and t_{fw}. Therefore, larger peak currents increase the transformer losses and would have to be switched-off by the two input switches, which also results in a larger heat sink and lower power density. In addition, the required number of secondary windings would increase from four to eight, if the same blocking voltage of the diodes is assumed. However, the number of diodes would be the same, since each output rectifier of the full-bridge requires two diodes compared to one diode for the flyback converter.

B. Experimental Results

Three experimental tests consisting on turn-off behavior, current sharing and nominal operation are now displayed to validate the converter design discussed in the previous sections.

1) IGBT turn-off behavior: One of the most critical transitions within the converter's operation is found when the current in the series inductor L_s is switched to freewheeling (t_{fw} in Fig. 3), where the peak current must be switched-off by one of the IGBTs.

TABLE III: Characteristics of the optimized full-bridge and the flyback converter.

Parameter	Full-bridge	Flyback
Maximum primary RMS current $I_{p,rms}$	58 A	66 A
Maximum primary peak current $\hat{I}_p$	151 A	202 A
Maximum IGBT losses	250 W	421 W
Maximum output diodes losses	71 W	55 W
Turns ratio n	7	12
Maximum primary copper losses	63 W	42.92 W
Maximum secondary copper losses	48 W	41 W
Maximum core losses	96 W	223 W
Number of cores pairs N_{set}	4+1	12
Transformer volume	0.63 dm^3	1.5 dm^3
Secondary windings	4	8
Minimum efficiency	96.2 %	93.2 %

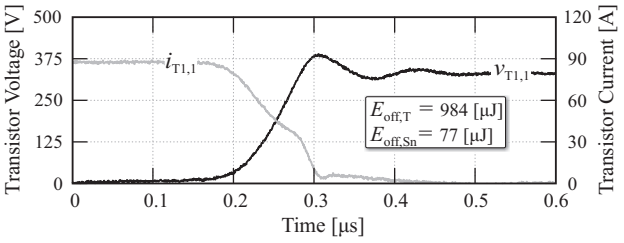

Figure 11: IGBT turn-off behavior: **(a)** Transistor $T_{1,1}$ current $i_{T1,1}$ and voltage $v_{T1,1}$; **(b)** Instantaneous dissipated power in IGBT, $p_{T1,1}$, and in IGBT snubber $p_{Sn1,1}$ during switching.

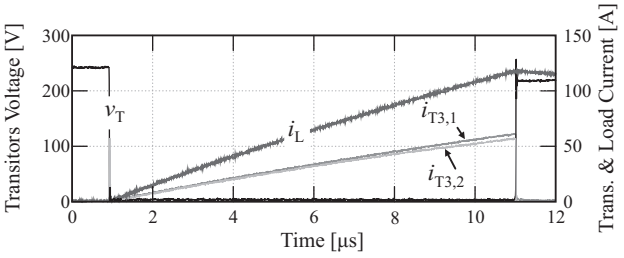

Figure 12: Current in two paralleled IGBTs: Transistor collector-emitter voltage v_T, load current i_L and current through paralleled IGBTs $i_{T3,1}$, $i_{T3,2}$.

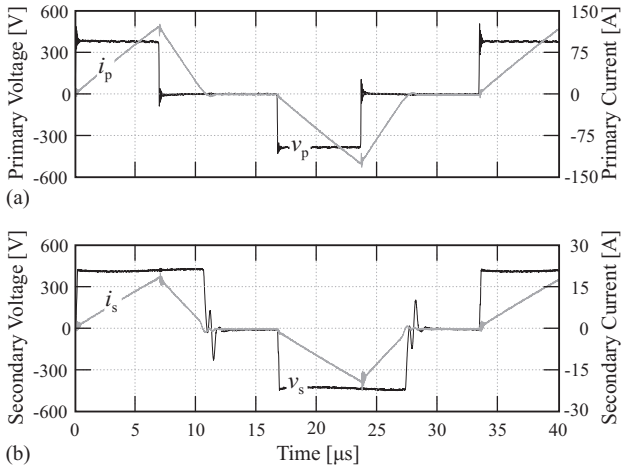

Figure 13: Experimental nominal behavior: **(a)** Primary voltage and current; **(b)** Voltage and current of one secondary.

In this case, to avoid overvoltages during the switching, RC snubber circuits where placed in each of the IGBTs, which also contribute to a reduction of 32 % in the overall switching losses.

The switching behavior of the selected IGBTs is shown in Fig. 11-a) for an inductive load of 220 µH conducting 80 A when the switching takes place. As can be seen, a fast switching with a 17.8 % overshoot is achieved where the energy dissipated in each turn-off process is $E_{off,T}$=984 µJ and $E_{off,Sn}$=77 µJ for the transistor and the snubber respectively. With these values, the maximum experimental turn-off losses reach $P_{Toff,e}$=127.3 W, whereas the theoretically calculated turn-off losses are $P_{Toff,t}$=138.6 W.

2) Current sharing: An important feature to be tested is the current sharing of the paralleled IGBTs of the input full-bridge. The test circuit consists on a inductive load L_s=220 µH connected in parallel to transistors $T_{1,1}$ and $T_{1,2}$ (cf. Fig. 4) leaving the rest of the converter unconnected. During a time duration of t_{on}=100 µs, the lower transistors $T_{3,1}$ and $T_{3,2}$ are switched on, applying the full input voltage to the load inductor. After this time, the current switches to $T_{1,1}$ and $T_{1,2}$ antiparallel diodes, where it freewheels until it decays to zero.

The result of the test is shown in Fig. 12. It can be seen that, as a result of the applied voltage (250 V), the current in the load rises linearly up to $\hat{i}_L$=118 A. The peak current conducted by transistor $T_{3,1}$ is $i_{T3,1}$ = 61.3 A and $i_{T3,2}$ = 56.6 A for transistor $T_{3,2}$. This values represent a 7.26 % relative difference in the current sharing, which is acceptable for the normal operation of the converter.

3) Nominal operation: In Fig. 13 the experimental result for an input and output voltage of $V_{in} = 400$ V and $V_{out} = 3500$ V at an output power of $P_{out} = 11$ kW is shown, where waveforms in Fig. 13-b) are measured from one of the four secondaries of the transformer.

As can be seen, the current and voltage waveforms at the primary follow closely the behavior described in Fig. 3. Under these nominal conditions, the peak current reached is $\hat{i}_p$=127 A and the voltage amplitude measured in one secondary is 438 V. Both values can be verified in the displayed results. Here it can be seen that the secondary currents and voltages suffer from oscillations when the current reaches zero, which are mainly due to the reverse recovery effects and junction capacitances of the output diodes.

VI. Conclusion

In this paper the operation, design, optimization and testing of a 3.5 kV/11 kW isolated full-bridge based DC-DC converter is presented. There, a complete model of the converter, focused on the transformer design, efficiency-volume optimization and component selection, was carried out. For the design of the transformer a special cooling concept is incorporated, due to the high output voltage and the needed isolation. Additionally, in order to obtain a high power density (1.54 kW/dm^3) the needed series inductance L_s of the converter is partly integrated into the transformer. With the presented design, a theoretical efficiency of 97 % is achieved. The efficiency and the power density of the converter were affected by the given operating range as each component was designed for a different operating point. As shown in the paper, compared to the well-known flyback converter, the proposed full-bridge based topology results in a much higher efficiency and power density.

References

[1] D. Bortis, S. Waffler, J. Biela, and J. W. Kolar, "25kW 3-phase unity power factor buck boost rectifier with wide input and output range for pulse load applications," in *Proc. 16th IEEE International Pulsed Power Conference*, vol. 2, 17–22 June 2007, pp. 1505–1508.

[2] F. Wang, A. Kuthi, and M. A. Gundersen, "Compact high repetition rate pseudospark pulse generator," vol. 33, no. 4, pp. 1177–1181, Aug. 2005.

[3] J. Elmes, C. Jourdan, O. Abdel-Rahman, and I. Batarseh, "High-voltage, high-power-density DC-DC converter for capacitor charging applications," in *Proc. Twenty-Fourth Annual IEEE Applied Power Electronics Conference and Exposition APEC 2009*, 15–19 Feb. 2009, pp. 433–439.

[4] J. Biela, U. Badstuebner, and J. W. Kolar, "Design of a 5-kW, 1-U, 10-kW/dm^{3}resonant DC-DC converter for telecom applications," vol. 24, no. 7, pp. 1701–1710, July 2009.

[5] U. Badstuebner, J. Biela, and J. W. Kolar, "Power density and efficiency optimization of resonant and phase-shift telecom DC-DC converters," in *Proc. Twenty-Third Annual IEEE Applied Power Electronics Conference and Exposition APEC 2008*, 24–28 Feb. 2008, pp. 311–317.

[6] K. Venkatachalam, C. R. Sullivan, T. Abdallah, and H. Tacca, "Accurate prediction of ferrite core loss with nonsinusoidal waveforms using only steinmetz parameters," in *Proc. IEEE Workshop on Computers in Power Electronics*, 3–4 June 2002, pp. 36–41.

[7] K. A. Alberto Guerra and S. Fimiani, "Ultra-fast recovery diodes meet todays requirements for high frequency operation and power ratings in smps applications," International Rectifier, Tech. Rep., 2000.

[8] C. R. Sullivan, "Optimal choice for number of strands in a litz-wire transformer winding," vol. 14, no. 2, pp. 283–291, March 1999.

[9] D. Aggeler, J. Biela, and J. W. Kolar, "A compact, high voltage 25 kW, 50 kHz DC-DC converter based on sic jfets," in *Proc. Twenty-Third Annual IEEE Applied Power Electronics Conference and Exposition APEC 2008*, 24–28 Feb. 2008, pp. 801–807.

[10] E. R. and M. D., *Fundamehntals of Power Electronics*. Springer Science+Business Media, LLC, 2001.

Jürgen Biela (S'04 M'06) received the Diploma (with honors) in electrical engineering from the Friedrich-Alexander University, Erlangen, Germany, in 2000, and the Ph.D. degree in electrical engineering from the Swiss Federal Institute of Technology (ETH), Zürich, Switzerland, in 2005. In the course of hisM.Sc. studies, he dealt in particular with resonant dc-link inverters at Strathclyde University, Glasgow, U.K., (term project) and the active control of seriesconnected integrated gate commutated thyristors at the Technical University of Munich, Munich, Germany, (Diploma thesis). In July 2002, he joined the Power Electronic Systems (PES) Laboratory, ETH Zürich, working toward the Ph.D. degree, concentrating on an optimized electromagnetically integrated resonant converter. He was with the Research Department, A&D Siemens, Germany, from 2000 to 2001, where he focused on inverters with very high switching frequencies, SiC components, and electromagnetic compatibility. From 2006 to 2007, he was a Postdoctoral Fellow with PES and has been a Guest Researcher at the Tokyo Institute of Technology, Tokyo, Japan. Since 2007, he has been a Senior Research Associate with PES, Electrical Engineering Department, ETH Zürich. His current research interests include multidomain modeling, design and optimization of PES, particularly systems for future energy distribution and pulsed power applications, advanced PES based on novel semiconductor technologies, and integrated passive components for ultracompact and ultraefficient converter systems.

Gabriel Ortiz was born in Chuquicamata, Chile, on September 13, 1984. He studied Electronics Engineering at Universidad Técnica Federico Santa María, Valparaíso, Chile, joining the power electronics group early on 2007. During his Master Thesis he worked with reconfiguration of regenerative and non-regenerative cascaded multilevel converters under fault condition, obtaining maximum qualification on his Thesis Examination. He received his M.Sc. degree in December 2008, and he has been a Ph.D. student at the Power Electronic Systems Laboratory, ETH Zürich, since February 2009.

Johann W. Kolar (M'89 SM'04) received the Ph.D. degree (summa cum laude/promotio sub auspiciis praesidentis rei publicae) from the University of Technology Vienna, Austria. Since 1984, he has been an Independent International Consultant in close collaboration with the Vienna University of Technology, in the fields of power electronics, industrial electronics, and highperformance drives. On February 1, 2001, he was appointed as a Professor and Head of the Power Electronic Systems Laboratory, Swiss Federal Institute of Technology (ETH), Zürich, Switzerland. He has proposed numerous novel PWM converter topologies, and modulation and control concepts, e.g., the VIENNA rectifier and the threephase ac-ac sparse matrix converter. He has published over 300 scientific papers in international journals and conference proceedings. He is the holder of 75 patents. His current research is on ac-ac and ac-dc converter topologies with low effects on the mains, e.g., for power supply of telecommunication systems, more electric aircraft, and distributed power systems in connection with fuel cells. His other main areas of research include the realization of ultracompact intelligent converter modules employing latest power semiconductor technology (SiC), novel concepts for cooling and EMI filtering, multidomain/multiscale modeling and simulation, pulsed power, bearingless motors, and power MEMS. Dr. Kolar is a member of the Institute of Electrical Engineers of Japan (IEEJ) and the technical program committees of numerous international conferences in the field (e.g., Director of the Power Quality Branch of the International Conference on Power Conversion and Intelligent Motion). From 1997 to 2000, he served as an Associate Editor of the "IEEE TRANSACTIONS ON INDUSTRIAL ELECTRONICS", and since 2001, as an Associate Editor of the "IEEE TRANSACTIONS ON POWER ELECTRONICS". Since 2002, he has been an Associate Editor for the Journal of Power Electronics of the Korean Institute of Power Electronics and a member of the Editorial Advisory Board of the IEEJ Transactions on Electrical and Electronic Engineering. He was the recipient of the Best Transactions Paper Award of the IEEE Industrial Electronics Society in 2005 and an Erskine Fellowship from the University of Canterbury, New Zealand, in 2003. In 2006, the European Power Supplies Manufacturers Association awarded the Power Electronics Systems Laboratory of ETH Zürich as the leading academic research institution in Europe.

Dominik Bortis (S'06) was born in Fiesch, Switzerland on December 29, 1980. He studied electrical engineering at the Swiss Federal Institute of Technology (ETH) Zurich. During his studies he majored in communication technology and automatic control engineering. In his diploma thesis he worked with the company Levitronix, where he designed and realised a galvanic isolation system for analog signals. He received his M.Sc. degree in May 2005, and he has been a Ph.D. student at the Power Electronic Systems Laboratory, ETH Zürich, since June 2005. After he finished his Ph.D in December 2008 he is now working as PostDoc at the PES, ETH Zurich.